Available online at www.sciencedirect.com

ScienceDirect

Advances in Space Research xxx (xxxx) xxx

ADVANCES IN SPACE RESEARCH (a COSPAR publication)

www.elsevier.com/locate/asr

Fuel-optimal acquisition and control of a cartwheel formation in Earth displaced heliocentric orbit

Stefano Marmori, Alessandro Morselli *

Politecnico di Milano, Dept. Aerospace Science and Technology, Via La Masa 34, 20156, Milan, Italy

Received 5 February 2024; received in revised form 17 August 2024; accepted 29 August 2024

Abstract

An optimization approach for cartwheel formation acquisition and maintenance in an Earth Displaced heliocentric orbit is presented. This work considers non-gravitational perturbations such as solar radiation pressure, thus extending the studies previously performed for the mission LISA. The problem is tackled as a Nonlinear Programming problem using a multiple shooting method. The optimization process is performed in two steps: first, the orbital elements of each satellite in heliocentric orbit are optimized to guarantee the stability during the science phase hence easing maintenance of the cartwheel formation in presence of orbital perturbations. Then, the obtained initial states are propagated to obtain a set of target orbital states which become the final target of a second optimization covering the transfer phase from Earth. For the science phase optimization presents two alternative cost functions are introduced, one based on the arm-length evolution and one on the arm-length-rate evolution. The performance of each cost function is analysed for different initial displacement angles: for target arm-lengths below 2.5 million kilometers the arm-length cost function provides the best results while no significant difference between the two optimized solutions is observed above this value. The transfer phase optimization presents two different approaches, one considering an injection on a trajectory more favourable for one of the three spacecraft and one considering an injection on an intermediate trajectory which minimizes the overall acquisition cost of all spacecraft. The proposed optimization approach performance are studied on a set of test cases covering both transfer and science phase, showing that stable configuration conditions can be found even in presence of orbital perturbations and that the multiple injection transfer is capable of providing a more homogeneous fuel consumption among the three spacecraft.

Keywords: Cartwheel formation flying; Trajectory design; Earth displaced heliocentric orbits

1. Introduction

The field of space exploration is constantly seeking to strike a balance between making ground-breaking technological and scientific discoveries and the demand for cost-effective solutions. In recent decades, formation flying missions have emerged as a way to reconcile these conflicting demands, offering, generally, a low-budget alternative while delivering innovative results. Formation flying (FF) can be defined as a multi-satellite mission in which a desired relative attitude and position between the spacecraft is maintained stable or actively controlled (Alfriend et al., 2010a). The main advantage is the possibility of dividing the functions of a single spacecraft between the elements composing the formation, improving reliability of the system. For instance, in the event of technical issues affecting one of the satellites, it might be possible for the other elements of the formation to compensate or mitigate such failures, thus ensuring continuation of the operations (Liu and Zhang, 2018). For homogeneous formations

* Corresponding author.
E-mail addresses: stefano.marmori@mail.polimi.it (S. Marmori), alessandro.morselli@polimi.it (A. Morselli).

https://doi.org/10.1016/j.asr.2024.08.073
0273-1177/

(Le Moigne et al., 2020), i.e, whenever the architecture of the spacecraft which make up the formation is the same, the production and testing phase can be simplified, reducing the cost as compared to a monolithic system (Sabol et al., 2001). Additionally, FF missions have the potential to deliver high technological and scientific returns by enabling the achievement of high-precision results, as well as offering the possibility of measuring and detecting phenomena that would not be possible with a single satellite. These missions have found extensive application in both scientific research and technological development. In the scientific category, notable missions include ESA's CLUSTER (Escoubet et al., 2001) and ESA/NASA GRACE (Tapley, 2008), which have demonstrated the significant benefits offered by this technology. Furthermore, ESA-supervised mission like PRISMA (Prototype Research Instruments and Space Mission Technology Advancement) (Gill et al., 2007) and PROBA-3 (Project for On-Board Autonomy-3) (Contreras et al., 2017), set to be launched in 2024, have contributed respectively to the advancement of FF by validating algorithms, sensors and actuators and the demonstration of precise formation flying capabilities. The effect of perturbations on formations in Earth orbit was analysed and schemes that make use of impulsive manoeuvres for multiple spacecraft formation-keeping using relative-orbital-element corrections were proposed (Beigelman and Gurfil, 2008). More recently, the case of formations flying around asteroids was studied and optimal control strategies based on indirect optimization methods for continuous low-thrust were devised (Wang et al., 2021). Also in this case the effect of perturbations is relevant since these bodies are characterised by irregular shapes and heterogeneous density.

Scheduled for launch in 2035 as part of the ESA Cosmic Vision 2015–2025 plan, the Laser Interferometer Space Antenna (LISA) is a mission that holds great promise for advancements in both scientific and technological domains. Extensive studies have been conducted for decades on this mission, ranging from preliminary investigations (Folkner et al., 1997; Danzmann, 1996) to recent developments (Amaro-Seoane et al., 2017), resulting in changes to the mission architecture. LISA aims to detect and measure gravitational waves with frequencies ranging from 0.1 mHz to 1 Hz (Colpi et al., 2024). Experiments at such low frequencies are problematic on Earth due to local fluctuating gravitational gradients and seismic waves, therefore the need to perform such experiments in space (Pitkin et al., 2011). The formation adopted for this mission is known as the cartwheel formation, which is comprised of n satellites evenly distributed on an ellipse centred on the formation's centre. In the case of LISA, three identical satellites orbit the Sun in a trailing or leading Earth Displaced Heliocentric Orbit (EDHO) with a distance from Earth between 50 and 65 million km and an inter-satellite distance of 2.5 million km. The entire mission can be divided into two phases. The first stage involves transferring the fleet from Earth to the final EDHO (Joffre et al., 2018; Yang et al., 2023), while the second phase encompasses acquiring the desired formation within the prescribed requirements on arm length L (relative distance between satellites), arm length rate $\dot{L}$ (relative velocity between satellites), and corner angle α (angle between formation arms) (Joffre et al., 2021; Xie et al., 2023; Yang and Zhang, 2019). A unique characteristic of this mission is that the Test Masses are shielded from non-gravitational forces, while Solar Radiation Pressure (SRP) acting on the surrounding spacecraft is counteracted by the Drag-Free Attitude Control System (DFACS). The DFACS is instrumental to the measurement performance for LISA, but the resulting assumption, i.e., the compensation of non-gravitational accelerations, limit the applicability of these analysis to the specific case of LISA.

Contrary to the planetary case, formation flying missions in deep space are characterised by the absence of perturbation sources like drag and non-spherical gravity, and in the case of LISA by large distance scale. The coupling between the different dynamics is achieved only by the presence of constraints (e.g., relative measurements) and by the definition of an objective function. Therefore it is possible to actively control each single spacecraft (Smith and Hadaegh, 2005; Schaub and Alfriend, 2001) in order to maintain the required relative position and velocity among the fleet to preserve the formation. Alternatively, a simpler approach involves optimizing the initial conditions to control the formation. This strategy has been widely adopted in numerous studies on LISA-like formations to mitigate or completely avoid noise effects resulting from thrust correction manoeuvres during the operational phase. Additionally, it reduces the possibility of outages, which would necessitate the re-acquisition of the laser links.

This paper aims to examine the potential impact of a different dynamic environment on the evolution of a heliocentric cartwheel formation with orbital characteristics similar to that of LISA (Martens and Joffre, 2021; Xia et al., 2010) and assess the formation stability in a dynamic environment that includes SRP perturbations. The inclusion of non-gravitational perturbations is a necessary step to enable the design of future missions with diverse scientific requirements and payloads. Less stringent constraints on the relative orbit control are present in such cases and, therefore, it is not necessary to actively compensate such perturbations as in the case of LISA. One example is the proposed ALBATROS mission, which employs heliocentric cartwheel formation to assess the intensity and the origin high-energy events with particular attention on obtaining a substantial sample of Gamma Ray Burst (Burderi et al., 2022). This is accomplished by undertaking a preliminary mission design that analyzes both the transfer and science phases. The transfer phase is explored through direct transfer strategies, while the science phase focuses on avoiding control manoeuvres during the operational stage. This work focuses on the case of small

satellites, with mass ranges between 500 kg and 1000 kg which have been proposed for different FF missions (Bandyopadhyay et al., 2016). Note that the constraint on the maximum mass affects in turn also the available fuel mass, hence it is desirable to study orbits strategies that limit the need of control manoeuvres yet preserving the desired relative configuration. In a cartwheel formation the geometry is not static, as the values of L, $\dot{L}$, and α change over time, resulting in a breathing motion. The objective of optimizing the initial conditions is therefore to stabilize the formation and minimize this phenomenon. Previous studies have approached the problem analytically, achieving reduced flexing by slightly tilting the formation plane (Nayak et al., 2006), while others have developed numerical optimization routines by establishing relations between the geometry and the relative orbital elements (ROE) (D'Amico et al., 2009). To summarize, this works aims at: (1) generalizing the approach to heliocentric cartwheel formations, extending the methodologies and optimizations used in LISA to a broader context where the active compensation of the SRP is not necessary, hence treating it as an additional perturbation to be accounted for in simulations; (2) introducing an optimization strategy, specifically designed for the science phase, to ensure formation stability and maintain accuracy; (3) introducing optimization approaches for the transfer phase to the science orbit considering impulsive manoeuvres and a single launch.

This paper is organized as follows. First, an overview of the cartwheel orbital elements and their relationships is given in Section 2, along with the definition of the dynamic environment and the new requirements on the geometry. In Section 3, the optimization problem is presented, addressing the stability of the formation, and the results are compared using two different cost functions for various initial conditions obtained changing the arm length and the initial displacement angle. Moving on to the transfer phase, a critical step involves deploying the three spacecraft into their pre-optimized orbits. Given the smaller mass of the satellites considered, strategies involving a single launch are possible. In such cases, the transfer process can be simplified into two phases. The first phase involves the injection of all satellites into the same transfer orbit by a single launcher. The second phase entails the subsequent independent trajectories of the satellites. Section 4 delves into two distinct strategies for releasing the vehicles, one with a single separation event for all three spacecraft and one with different separation epochs. Section 5 provides a comparative analysis of the two transfer approaches and the corresponding results, providing considerations in terms of fuel mass distribution among the three spacecraft. Finally, the work concludes with Section 6, encompassing the study's conclusions and potential path for future development.

2. Cartwheel formation

In this section a brief overview of the technical background of the cartwheel formation problem is provided. First, the definition of the keplerian elements and their relationship in the case of unperturbed motion is provided. Then, an analysis of the effect of the main perturbation sources like gravitational attraction from other celestial bodies and solar radiation pressure is analysed to assess the more relevant perturbations for the analysed case. Finally, the target cartwheel formation considered in this study is outlined in terms of target geometrical parameters such as arm length, arm length rate and corner angle and their allowed deviations.

2.1. Keplerian orbital elements representation

The first step in further analysing the problem is to define the cartwheel formation using orbital elements. This requires studying the relative motion between satellites, particularly the motion of a deputy with respect to another spacecraft or fictitious point referred as to chief. In the case of a heliocentric cartwheel formation the chief is the center point of the formation orbiting on the ecliptic, while there are three deputy satellites orbiting with a circular motion the center, forming an equilateral triangle. Some key simplifications can be made in order to simplify the analysis. First, to prevent significant drift of the formation with respect to Earth, the semi-major axis of the chief must be approximately equal to 1 AU and it must follow a near-circular orbit. Additionally, it is worth noticing that the relative distance between the chief and the deputy is small compared to the distance between the primary body and the chief; therefore, it is possible to use a first-order model to describe the approximate relative motion known as the Clohessy-Wiltshire equations (Clohessy and Wiltshire, 1960), that are expressed in the magnitude-phase form as follow:

$$x(t) = \rho_x \sin(nt + \alpha_x) \tag{1}$$

$$y(t) = \rho_y + 2\rho_x \cos(nt + \alpha_x) \tag{2}$$

$$z(t) = \rho_z \sin(nt + \alpha_z) \tag{3}$$

The relative motion between the satellites can be geometrically characterized by setting up some relations between the integration constants $\rho_x, \rho_y, \rho_z, \alpha_x$, and α_z displayed in Eq. (1), which are all function of Cartesian coordinates (D'Amico and Montenbruck, 2006). The relative circular motion of the three satellites can be obtained through a particular orbit referred to as General Circular Orbit (GCO) that can be defined by setting $\alpha_x = \alpha_z$ and $\rho_z = \sqrt{3}\rho_x$ (Alfriend et al., 2010b). The next step involves moving the description of the relative motion from Cartesian coordinates to a set of Relative Orbital Elements

(ROE), which defined as function classical orbital elements as follows:

$$\delta\boldsymbol{\alpha} = \begin{pmatrix} \delta a \\ \delta\lambda \\ \delta e_x \\ \delta e_y \\ \delta i_x \\ \delta i_y \end{pmatrix} = \begin{pmatrix} (a^{(j)}) - a_0)/a_0 \\ (u^{(j)} - u_0) + (\Omega^{(j)} - \Omega_0)\cos i_0 \\ e_x^{(j)} - e_{x0} \\ e_y^{(j)} - e_{y0} \\ i^{(j)} - i_0 \\ (\Omega^{(j)} - \Omega_0)\sin i_0 \end{pmatrix} \tag{4}$$

where the subscript 0 refers to the chief orbit and the superscript j to a generic spacecraft of the formation. The vector is composed of the following elements: δa, the normalized semi-major axis difference, $\delta\lambda$, the relative mean longitude defined using the mean argument of latitude $u = \omega + M$ and the remaining quantities, which are the components of the eccentricity and inclination vectors. These components are expressed in the polar notation are the following:

$$\delta\boldsymbol{e} = \begin{pmatrix} \delta e_x \\ \delta e_y \end{pmatrix} = \delta e \begin{pmatrix} \cos\phi \\ \sin\phi \end{pmatrix} \tag{5}$$

$$\delta\boldsymbol{i} = \begin{pmatrix} \delta i_x \\ \delta i_y \end{pmatrix} = \delta i \begin{pmatrix} \cos\psi \\ \sin\psi \end{pmatrix} \tag{6}$$

where the relative perigee and relative ascending node are denoted as ϕ and ψ. To obtain the orbital elements of each satellite, it is essential to have a clear understanding of some aspects of the formation. The center follows a circular heliocentric orbit on the ecliptic at a distance of 1 AU meaning that $a_0 = 1$ AU, $e_0 = 0$, and $i_0 = 0$. Additionally, the center needs to be displaced from Earth at a specific angle called *displacement angle* (Θ_0). This angle is determined as the difference between the heliocentric mean longitude of the center and the mean Earth, expressed as $\Theta_0 = l_0 - l_{ME}$ where $l = \omega + M + \Omega$. It is worth noticing that this definition differs from the one used in some other studies, such as (Joffre et al., 2021), where the mean Earth-Moon barycentre is taken as the reference instead of the mean Earth. A graphical representation of the cartwheel formation is given in Fig. 1.

To ensure that the cartwheel formation remains stationary with respect to Earth, is necessary to maintain the relative semi major axis (δa) equal to zero, which results in:

$$a^{(j)} = 1\text{AU} \tag{7}$$

By considering the first GCO relation between ρ_x and ρ_z and the nominal arm length, it is possible to establish a connection between the relative inclination and eccentricity, where $\delta i^{(j)} = \sqrt{3}\delta e^{(j)}$. This leads to the definition of the eccentricity of each spacecraft as:

$$\delta e^{(j)} = e^{(j)} = \frac{L}{2a_0\sqrt{3}} \tag{8}$$

$$i^{(j)} = \frac{L}{2a_0} \tag{9}$$

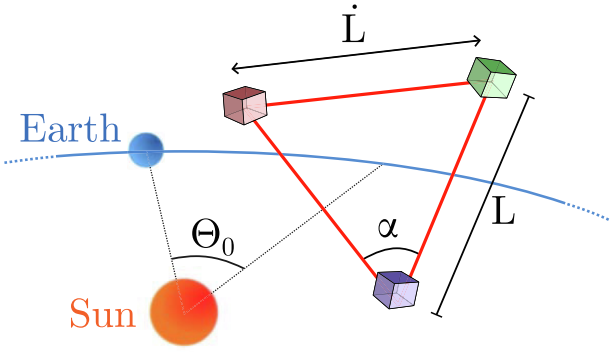

Fig. 1. Illustration of cartwheel parameters: Θ_0 being the displacement angle, while $L, \dot{L}$ and α are the arm length, arm length rate and corner angle respectively.

The second relation $\alpha_x = \alpha_z$ represents a perpendicularity condition between the relative eccentricity and inclination vector. From $i_0 = 0$, it follows that $\delta i_y = 0$ and by adding the perpendicularity condition, $\delta e_x = 0$ is obtained. This leads to only two values of the argument of perihelion that can satisfy this result

$$\omega^{(j)} = \frac{\pi}{2} \quad \text{or} \quad \omega^{(j)} = \frac{3\pi}{2} \tag{10}$$

These values define two types of cartwheel formations, which can be distinguished by looking at the motion of the cartwheel from the Sun: for $\omega = 3\pi/2$, the motion of the three satellites is clockwise, while for $\omega = \pi/2$, it is counter-clockwise (Fig. 2).

The final step to achieve the cartwheel formation involves distributing the three spacecraft on a circular orbit with a phase angle of $2\pi/3$, which can be accomplished by imposing conditions on either the RAAN or mean anomaly. For this study, the selected free parameter is the RAAN of the first satellite, while the RAANs of the other elements of the fleet can be obtained by adding or subtracting $2\pi/3$ from the first.

$$\Omega^{(1)} \in \mathbb{R} \tag{11}$$

$$\Omega^{(2)} = \Omega^{(1)} - 2\pi/3 \tag{12}$$

$$\Omega^{(3)} = \Omega^{(1)} - 4\pi/3 \tag{13}$$

Ultimately, the fleet assumes the desired configuration if all three spacecraft have the same initial mean longitude, defined by l_0.

$$M^{(1)} = l_0 - \omega^{(1)} - \Omega^{(1)} \tag{14}$$

$$M^{(2)} = M^{(1)} + 2\pi/3 \tag{15}$$

$$M^{(3)} = M^{(1)} + 4\pi/3 \tag{16}$$

2.2. Orbital perturbation analysis

The problem at hand is a complex optimization involving two interdependent phases: the transfer, from Earth to the desired heliocentric orbit and the science phase, in

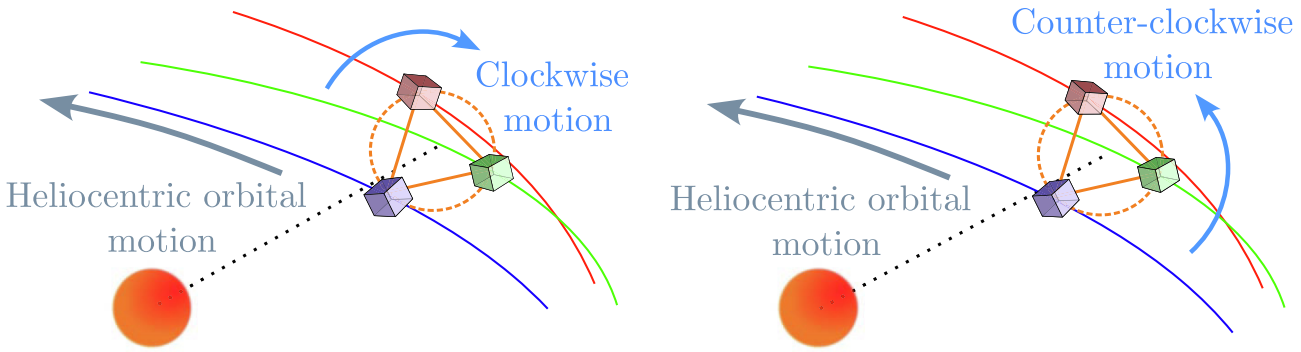

(a) Clockwise motion ($\omega = 3\pi/2$) (b) Counter-clockwise motion ($\omega = \pi/2$)

Fig. 2. Possible cartwheel formation mode depending on the selection of ω.

which the formation must satisfy the desired requirements. This paper presents a preliminary analysis of such problem wherein the two phases are optimized separately while considering the continuity between them. The dynamic environment in which the cartwheel formation is simulated takes into account the effects of solar radiation pressure and the gravitational influence of several celestial bodies, including the Sun, Mercury, Venus, Earth, Moon, Mars, Jupiter and Saturn. The selection of celestial bodies and the consideration of non-gravitational perturbations in this study are based on an analysis of the accelerations experienced by a satellite in an EDHO as function of the initial displacement angle. To maintain simplicity, circular orbits with radii equal to the semi-major axis are assumed for all bodies. The Earth and the Moon are displaced by an angle Θ_0 with respect to the test satellite, while all the other planets are aligned with it. The latter have two possible configurations: one where the spacecraft and the planet are the closest, resulting in the strongest gravitational pull, and another where the body is on the opposite side relative to the Sun, leading to the weakest attraction. These two solutions are combined to compute the average acceleration, resulting in a constant trend as function of Θ_0. The results, depicted in Fig. 3, demonstrate that Jupiter and Venus exhibit magnitudes of perturbations comparable to that of the Earth, depending on the displacement angle. Nevertheless, the Earth remains the most significant source of perturbation due to its relatively constant distance from the satellite, ensuring a continuous gravitational influence on the spacecraft dynamics. Uranus and Neptune, as well as the effects of non-spherical bodies are neglected due to their low perturbations and are not represented in the figure. Finally, it is worth noting that the intensity of the SRP perturbation is one of the most relevant, meaning that a more generalized analysis of the cartwheel formation is needed. For an area-to-mass ratio of 0.04 m^2/kg the SRP acceleration is larger than the one of the Earth for $\Theta_0 > 12$ deg.

The analysed formation shares the same geometry as that of LISA, allowing for the identification of any potential differences and similarities in the results obtained with these approaches as compared to previous studies. The nominal arm length is 2.5 million kilometers with an initial displacement angle of -20 degrees. A trailing configuration is selected since the transfer cost required for reaching this configuration is typically lower than that for acquiring Earth Leading Heliocentric Orbits (ELHOs). This is due to the fact that an increase of the aphelion requires a lower delta-V than an equivalent reduction of the perihelion. It is important to note, however, that the transfer cost is influenced by seasonal effects resulting from the Earth's eccentricity. When the Earth is closer to its heliocentric orbit perihelion, an ELHO may be more advantageous in terms of delta-V (Joffre et al., 2018).

2.3. Target cartwheel formation parameters

The study aims to address both the scientific and transfer phase concurrently. The former is presented in Section 3 and involves stabilizing the formation for a duration of 10 years, with the geometrical parameters satisfying the requirements outlined in Table 1. The reference parameters are taken from Burderi et al. (2022) and are also similar to those of LISA (Martens and Joffre, 2021). Instead of developing a control system to rectify relative orbits (Schaub and Alfriend, 2001), the approach here is to optimize the initial conditions of the operational phase, corresponding to the conclusion of the transfer. The primary aim of this study is to evaluate whether this strategy, widely adopted in numerous previous investigations (Joffre et al., 2021), can be effectively applied to heliocentric cartwheel formations influenced by Solar Radiation Pressure. To complete the framework, it is also essential to define a transfer phase. The goal is to propose various transfer strategies that directly align with the optimized initial orbital elements obtained in the science phase. As this analysis serves as a preliminary investigation, the simplest transfer scenario is considered: a direct transfer without Trajectory Correction Manoeuvres, in which the spacecraft are initially placed on a transfer trajectory by the launch vehicle and subsequently directed towards the final orbit using the onboard chemical propulsion system. Operationally, the transfer can be

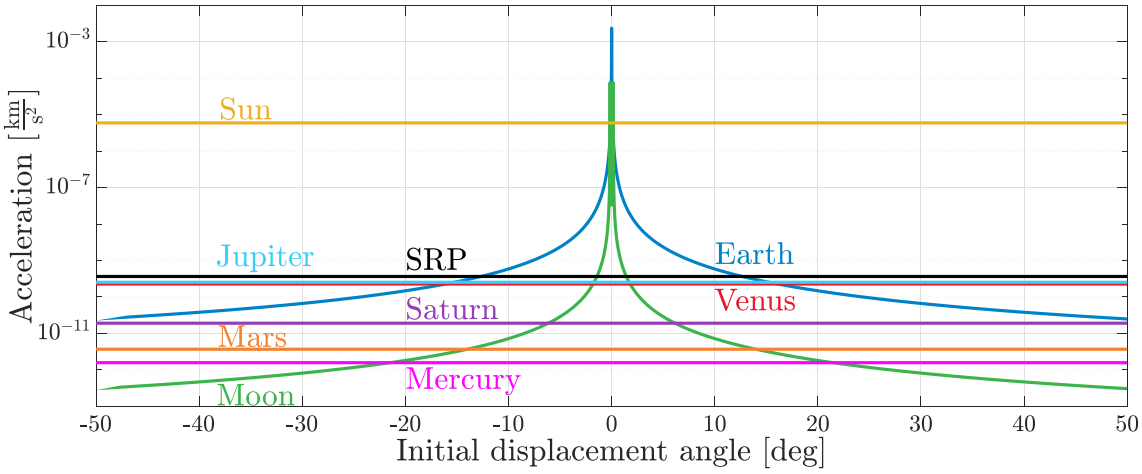

Fig. 3. Perturbations for different initial displacement angle for a spacecraft with area-to-mass ratio of 0.04 m^2/kg.

Table 1
Requirements on formation geometry.

Parameter	Requirement
Arm length	$L \in [2.45 \times 10^6, 2.55 \times 10^6]$ km
Arm length rate	$\dot{L} \in [-10, 10]$ m/s
Corner angle	$\alpha \in [58.8, 61.2]$ deg

divided into two phases. The first one involves the satellite remaining in close proximity after being injected into the same transfer trajectory by a launcher. The second phase involves the spacecraft individually manoeuvring towards their respective destinations. During the initial phase, assumptions are made to ignore conjunctions and close approaches between the satellites. A key requirement regarding the first part of the trajectory is the use of a single launch vehicle, which constrains all three spacecraft to follow a common escape trajectory.

2.4. Overview of the two-steps optimization framework

In this section a brief overview of the problem is given. The science and transfer phases of the formation are tackled through distinct yet interconnected optimization processes as detailed respectively in Section 3 and 4. The science phase focuses on optimizing the initial orbital elements to ensure a stable formation despite perturbations from SRP. The initial guessed orbital elements undergo a fine-tuning optimization to maintain the desired geometric configuration over an extended period. The transfer phase, on the other hand, aims to develop efficient strategies for transferring the spacecraft from Earth to the operational heliocentric orbit. By referencing the optimized initial conditions derived from the science phase, the transfer phase ensure that the spacecraft arrive in the correct configuration, ready to maintain the cartwheel formation. This approach underscores the importance of integrating both phases to achieve mission success. An overview of the combined optimization strategy is shown in Fig. 4.

Section 4 presents two distinct approaches to the release strategy, outlining a unified optimization problem capable of addressing both phases and provide a preliminary sizing of the transfer. The entire analysis is performed using GODOT[1], a flight dynamics software employed at ESOC used in this context for satellite propagation within the dynamic environment defined by gravitational and non-gravitational accelerations previously described. The optimization problems in this study were solved using PyGMO (Biscani and Izzo, 2020), leveraging its flexibility to handle complex orbital dynamics and its general focus on aerospace-related problems. User-defined problems were created utilizing NLopt solvers[2].

3. Science-phase optimization

3.1. Initial guess and natural evolution with perturbations

This section describes two different optimization techniques designed to ensure the stability of the cartwheel formation. The initial guess for the orbital elements used to define the cartwheel formation is presented in Table 2. These parameters provide a baseline for understanding the natural evolution of the formation under the influence of perturbations, such as SRP and gravitational forces from other celestial bodies. The non-optimized Keplerian formation serves as a starting point for the optimization. These orbital elements are chosen based on the theoretical model previously illustrated in Section 2, providing a reference configuration without any applied optimization techniques. The whole framework, both for the propagation and the optimization, is built using GODOT which gives different possibility for the available reference frames. In this study the EMCJ2000 (Mean Ecliptic of J2000) centered in the Solar System Barycenter is utilized to simulate the

[1] https://godot.io.esa.int/godotpy/ (Last accessed on February 04, 2024)
[2] Steven G. Johnson, The NLopt nonlinear-optimization package, http://github.com/stevengj/nlopt

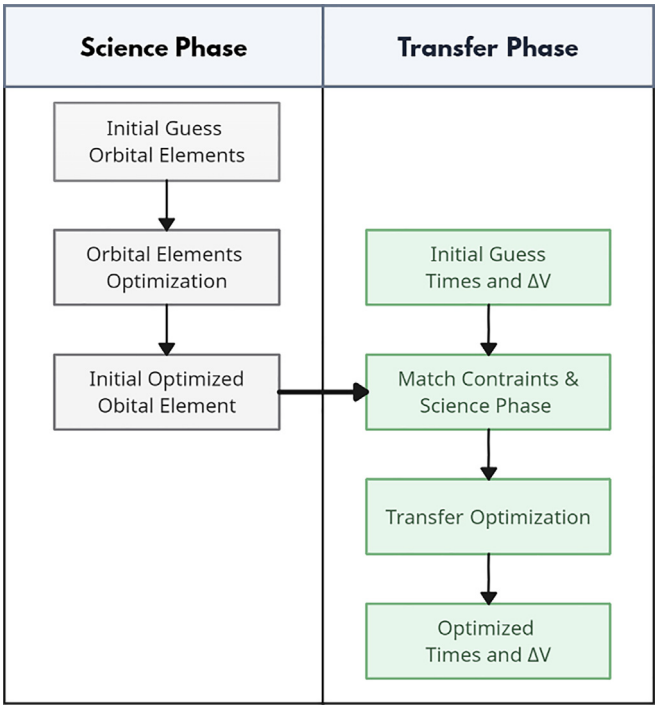

Fig. 4. Block diagram of the Science (light gray) and Transfer Phase (light green).

orbital dynamics. Regarding the ephemeris data, JPL DE432 was used, providing precise positions and velocities of celestial bodies.

For this analysis the maximum allowed variation from the reference value is set to 2% as shown in Table 1. By illustrating the three geometrical parameters of the non-optimized formation, it becomes evident that as the observation period progresses, the formation's parameters fail to meet the required limits (see Fig. 5). Therefore, the initial orbital elements must be adjusted to align with the defined requirements. This optimization aims to refine the initial parameters and enhance the stability of the formation, ensuring that it remains within acceptable bounds over extended periods.

3.2. Optimization strategies

The decision vector therefore comprises an initial time, corresponding to when the fleet achieves the desired geometry and the science phase starts, and three set of orbital elements.

$$\begin{aligned} &\boldsymbol{y} = \{t_0, \mathscr{K}_1, \mathscr{K}_2, \mathscr{K}_3\} \\ &\text{where } \mathscr{K}_j = \{a, e, i, \omega, \Omega, \theta\} \quad \text{with } j = 1, 2, 3 \end{aligned} \tag{17}$$

To maintain the required triangular equilateral shape, the cost function must be designed to increase its value whenever the formation deviates from the desired geometry. A continuous cost function can be defined to penalize the difference between the geometrical parameters, particularly the arm lengths (L) and the relative velocities ($\dot{L}$), leading the fleet towards an equilateral shape. On the other hand, a cost function based on corner angle (α) alone may not be adequate as it does not restrict the sides of the triangular formation. In this context, two distinct cost functions are employed, each offering an alternative approach to improve the formation stability. The first cost function minimizes variations in the side lengths of the triangular formation, promoting an equilateral configuration as defined by requirements. The second cost function targets the relative velocity of the satellites with the same aim as the first one, maintain the formation's shape. By applying these different cost functions, the study aims to identify the most effective method for optimizing the formation's stability under varying conditions, thereby providing a comprehensive assessment of potential optimization strategies. The two alternative cost functions selected for the optimization problem are the following:

$$J_{Length} = \int_{t_0}^{t_f} (L_1(t) - L_2(t))^2 + (L_1(t) - L_3(t))^2 \, dt \tag{18}$$

$$J_{Rate} = \int_{t_0}^{t_f} (\dot{L}_1(t) - \dot{L}_2(t))^2 + (\dot{L}_1(t) - \dot{L}_3(t))^2 \, dt \tag{19}$$

Overall, the initial keplerian orbital elements $\mathscr{K}_j$, where subscript j identifies each spacecraft, that minimize the breathing of the formation are obtained by solving one of the following NLP problem, which only differ by the choice of the cost function:

$$\begin{aligned} &\min_{\mathbf{y}} \mathrm{J}_{\mathrm{Length}} \quad \text{where} \mathbf{y} = \{t_0, \mathscr{K}_1, \mathscr{K}_2, \mathscr{K}_3\} \\ &\qquad \text{and} \mathscr{K}_j = \{a, e, i, \omega, \Omega, \theta\} \ \text{ with } j = 1, 2, 3 \end{aligned} \tag{20}$$

$$\begin{aligned} &\min_{\mathbf{y}} \mathrm{J}_{\mathrm{Rate}} \quad \text{where} \mathbf{y} = \{t_0, \mathscr{K}_1, \mathscr{K}_2, \mathscr{K}_3\} \\ &\qquad \text{and} \mathscr{K}_j = \{a, e, i, \omega, \Omega, \theta\} \quad \text{with } j = 1, 2, 3 \end{aligned} \tag{21}$$

The optimization procedure involves several steps, which are outlined in Algorithm 1 and Fig. 6 and can be summarized as follows. Firstly, an initial estimate of the three sets of orbital elements is obtained by fixing the geometry and position of the formation. These elements are subsequently converted into Cartesian coordinates and propagated for a duration of 10 years. The geometry parameters of the formation are computed based on these states and the values of L and $\dot{L}$ are determined at each step and used to calculate

Table 2
Non-optimized orbital elements for each spacecraft in EMCJ2000 reference frame.

	a [km]	e [-]	i [deg]	Ω [deg]	ω [deg]	θ [deg]
SC$_1$	149597870.7	0.0048241852	0.478748287	262.494884	90	87.8036189
SC$_2$	149597870.7	0.0048241852	0.478748287	142.494884	90	206.999515
SC$_3$	149597870.7	0.0048241852	0.478748287	22.4948843	90	326.950724

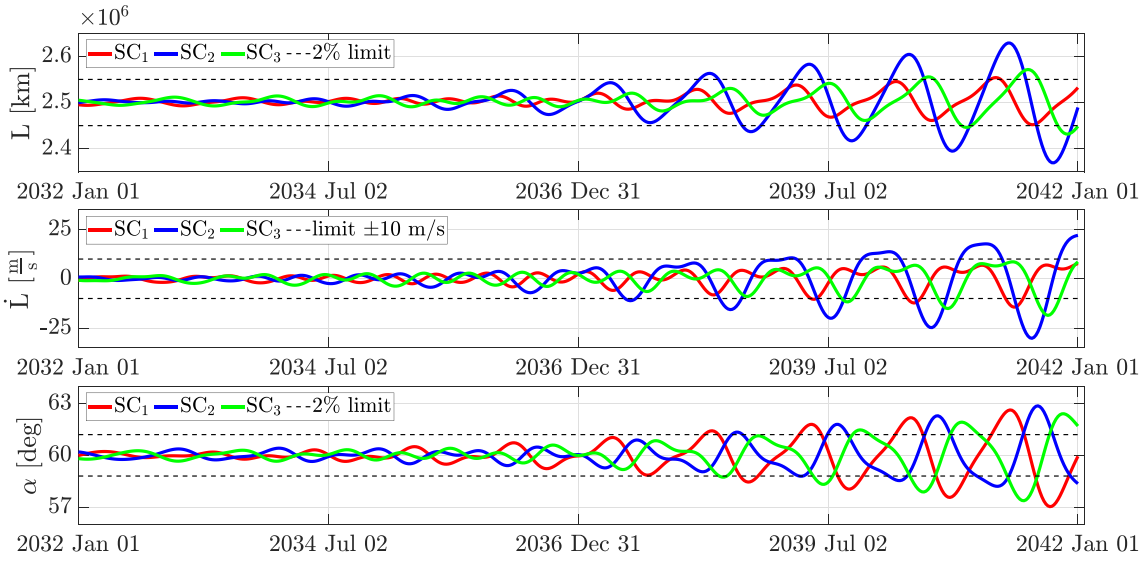

Fig. 5. Non optimized geometry evolution.

the cost functions. The last step of the algorithm involves solving the optimization problem to minimize the selected cost function, either J_{Length} or J_{Rate} defined in Eq. (18) and Eq. (19) respectively. The optimization itself refine these parameters, which are then propagated and then stored in OEM files for future utilization in the transfer analysis.

Algorithm 1. Science phase optimization algorithm

Algorithm 1: Science phase optimization algorithm

Data: $\Theta_0, \omega, L, t_0, t_f$
Result: Optimized initial keplerian elements
$\mathcal{K}_j = \{a, e, i, \omega, \Omega, \theta\}$ with $j = 1, 2, 3$
Set the values of Θ_0, ω, L, t_0 and t_f;
Compute the initial guessed orbital elements
$\mathcal{K}_1(t_0)$, $\mathcal{K}_2(t_0)$ and $\mathcal{K}_3(t_0)$ using equations in Section 2;
Create a vector of times t_i ranging from t_0 to t_f;
while *SLSQP not converged* **do**
  Convert the initial orbital elements to cartesian states
  $\mathbf{x}_1(t_0)$, $\mathbf{x}_2(t_0)$, $\mathbf{x}_3(t_0)$;
  for $t_i \in [t_0, ..., t_f]$ **do**
    Propagate the initial condition to obtain
    $\mathbf{x}_1(t_i)$, $\mathbf{x}_2(t_i)$, $\mathbf{x}_3(t_i)$;
    Compute the arm length $L_1(t_i)$, $L_2(t_i)$ and $L_3(t_i)$;
    Compute the arm length rate $\dot{L}_1(t_i)$, $\dot{L}_2(t_i)$ and
    $\dot{L}_3(t_i)$;
  end
  Compute the cost function J_{Length} (see Eq. 18) or
  J_{Rate} (see Eq. 19);
  Update the set of initial keplerian orbital elements
  $\mathcal{K}_1(t_0)$, $\mathcal{K}_2(t_0)$, $\mathcal{K}_3(t_0)$
end
Postprocessing:
Convert the optimal initial keplerian orbital elements to
cartesian states $\mathbf{x}_1(t_0)$, $\mathbf{x}_2(t_0)$, $\mathbf{x}_3(t_0)$;
Generate OEM orbit files covering the science phase
from t_0 to t_f;

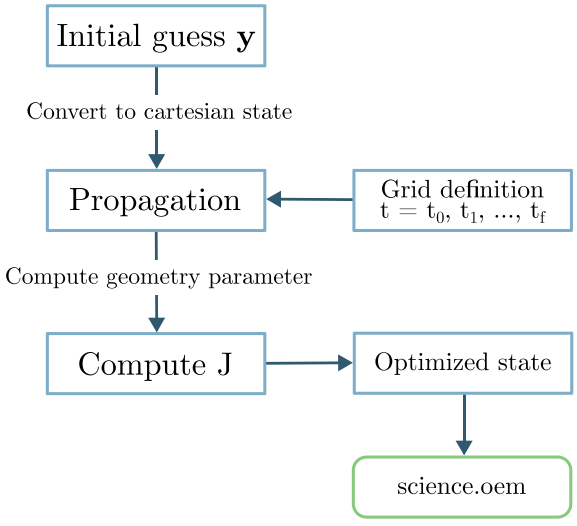

Fig. 6. Block scheme of the Science phase optimization inner loop.

3.3. Optimization results and performance analysis

The results of the optimization process were obtained using a gradient-based solver (SLSQP) from the NLOpt library and are reported in Table 3. This solver was selected because of the relative simplicity in calculating the gradient of the optimization problem under study. Fig. 7, which depicts the trends of the optimized geometrical parameters, demonstrates that the algorithm significantly enhances the stability and maintenance of the cartwheel formation, thereby ensuring that the configuration remains within the desired threshold over time.

Comparing the optimized with the non-optimized solution, it's clear that the natural evolution of the formation

Table 3
Optimized orbital element for each spacecraft in EMCJ2000 reference frame.

	a [km]	e [-]	i [deg]	Ω [deg]	ω [deg]	θ [deg]
SC_1	149597850.88079995	0.0048250157	0.4773054878	−97.6407370502	89.7337768625	87.5913867801
SC_2	149597502.72236753	0.0048253549	0.4837030658	142.4830979346	89.7300868309	−153.3335745242
SC_3	149598261.59946975	0.004824996	0.4785315545	22.5228723263	89.7318336074	−33.4234047893

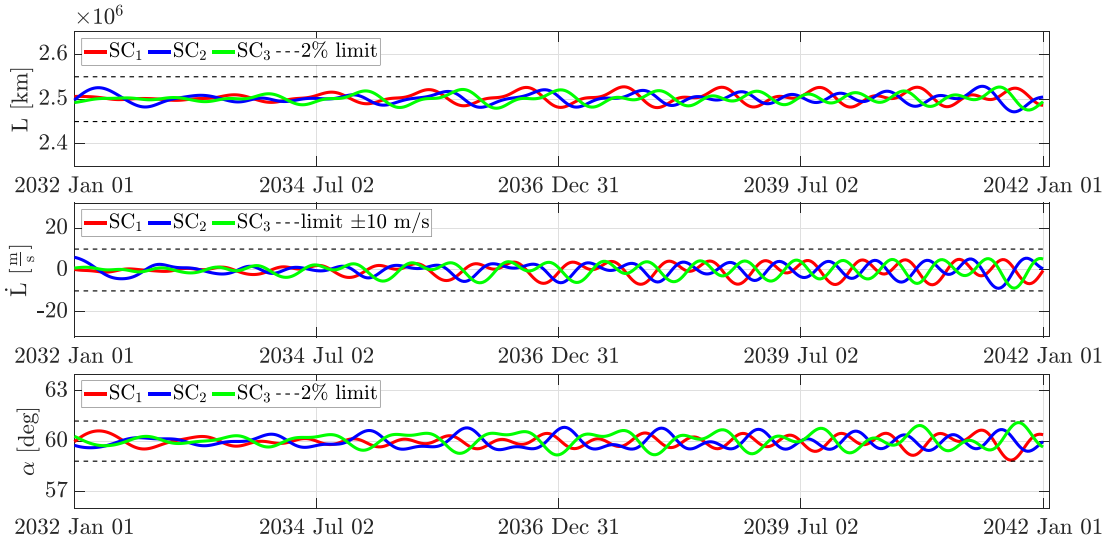

(a) Optimization results obtained with J_{Length}

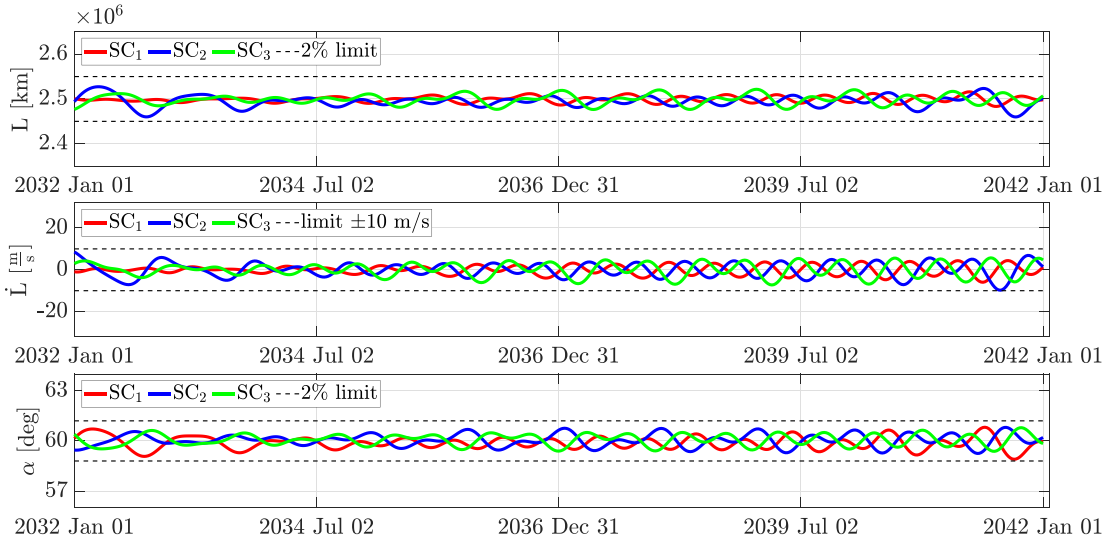

(b) Optimization results obtained with J_{Rate}

Fig. 7. Optimized geometrical parameters $L, \dot{L}$ and α for a cartwheel formation with $\Theta_0 = -20$ deg and $L = 2.5 \times 10^6$ km.

is significantly affected by the initial conditions. In the non-optimized case, the geometry initially appears closer to the nominal value. However, due to perturbations the formation quickly evolves beyond permissible bounds, exceeding the designated thresholds. Conversely, the implementation of optimized initial conditions, although potentially yielding inferior performance initially, guarantees the formation to remain within the prescribed boundaries throughout the entirety of the observation period. It is worth noting that the optimization framework allows tuning the time interval $[t_0;\ t_f]$ for controlling the formation geometrical parameters, hence it can be adapted to different mission scenarios. The duration of this time interval can therefore be shortened or increased depending on the mission requirements and expected science phase duration. These results are depicted in Figs. 7a and 7b, which respectively illustrate the outcomes of of J_{Length} and J_{Rate}. These two cost functions have been designed following previous studies

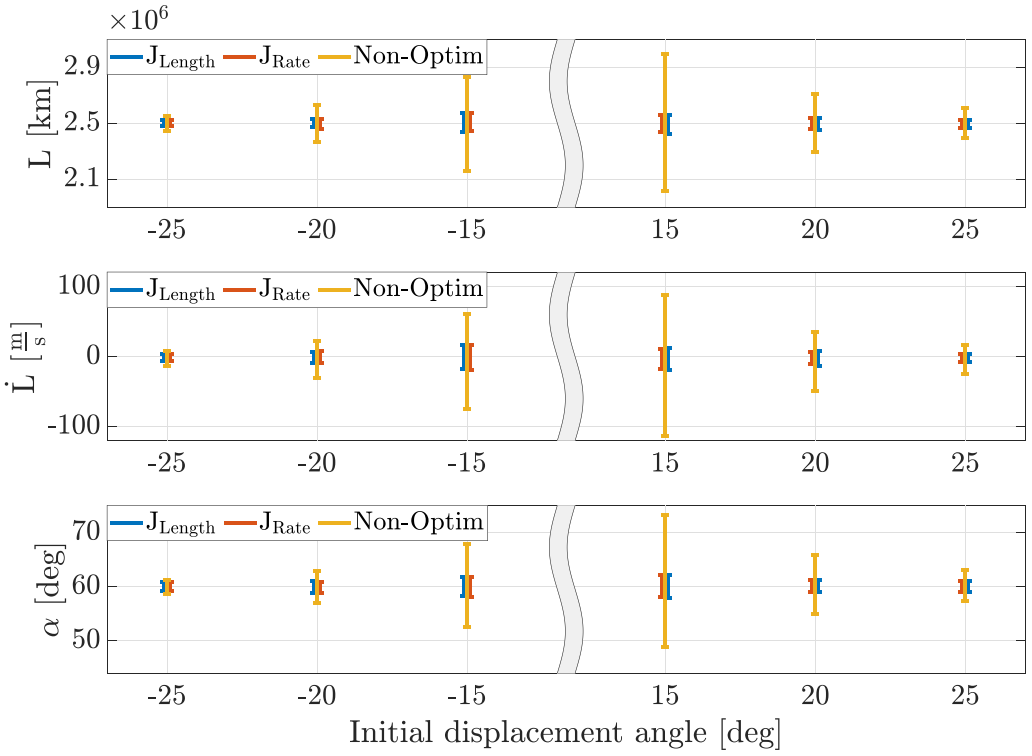

Fig. 8. Comparison in terms of parameters variations between optimized and non-optimized parameters for different initial displacement angles.

(Hughes and Bauer, 2002), with the aim of providing a rapid and straightforward implementation to assess whether the presence of SRP induces significant deviation from unperturbed scenarios. If a higher degree of stability is desired, more intricate cost functions can be employed, as demonstrated in (Xie et al., 2023). In that study, the formation design was achieved using two approaches: defining a multi-objective optimization problem and constructing a comprehensive cost function that incorporates all geometrical parameters (L, $\dot{L}$, and α) into a single index. In the presented case, after the optimization process, all requirements are satisfied within the specified time window, even in the presence of additional perturbations such as SRP. Both cost function exhibit similar behavior, necessitating further analysis to determine their effectiveness.

The investigation focuses on determining the maximum deviation of each geometrical parameter from its nominal value across various initial displacement angles and arm lengths, providing valuable insights into the behavior of the formation under different initial conditions. Firstly, the analysis is carried on for different initial displacement angles to identify any emerging trends resulting from placing the formation at different distanced from Earth. Fig. 8 displays the computed range of geometrical parameters using both optimized and non-optimized initial conditions. For larger angles, the optimization does not yields significant results as the perturbation caused by Earth is mitigated by the substantial distance between the celestial body and the formation's center. While higher initial displacement angles may enhance formation stability, they also lead to increased transfer costs and pose challenges for the communication subsystem. Notably, the optimization results are remarkably better for lower angles where Earth's influence is more significant, resulting in a substantial reduction in the range of each geometrical parameter.

However, this reduction alone is insufficient to meet the imposed requirements as depicted in Fig. 9, which focuses on the optimized results to analyze the behavior of the two cost functions. For higher angles, the optimization routine successfully ensure compliance with the requirements. Nevertheless, the solution with initial displacement angle of $|\Theta_0| = 20$ deg will be adopted as target operational orbit, following the approach employed in (Martens and Joffre, 2021). This particular solution offers an acceptable level of stability while keeping the transfer costs relatively low. Regarding the disparity between the two cost functions, no discernible trend identifies a consistently superior optimization approach. Similarly, the analysis is repeated for different arm lengths as illustrated in in Fig. 10. To accomplish this, the optimization routine outlined in Algorithm 1 is executed multiple times using different arm lengths, and the resulting solutions are obtained for the two previously described cost functions. These outcomes comprise the optimal initial conditions for various L values, which can be utilized to calculate the trajectory of the geometrical parameters over a 10-year time span. By comparing the maximum deviation from the nominal value for each geometrical characteristic, it is possible to determine the effectiveness of the two cost functions. A smaller difference indicates a better optimization of the formation. It is

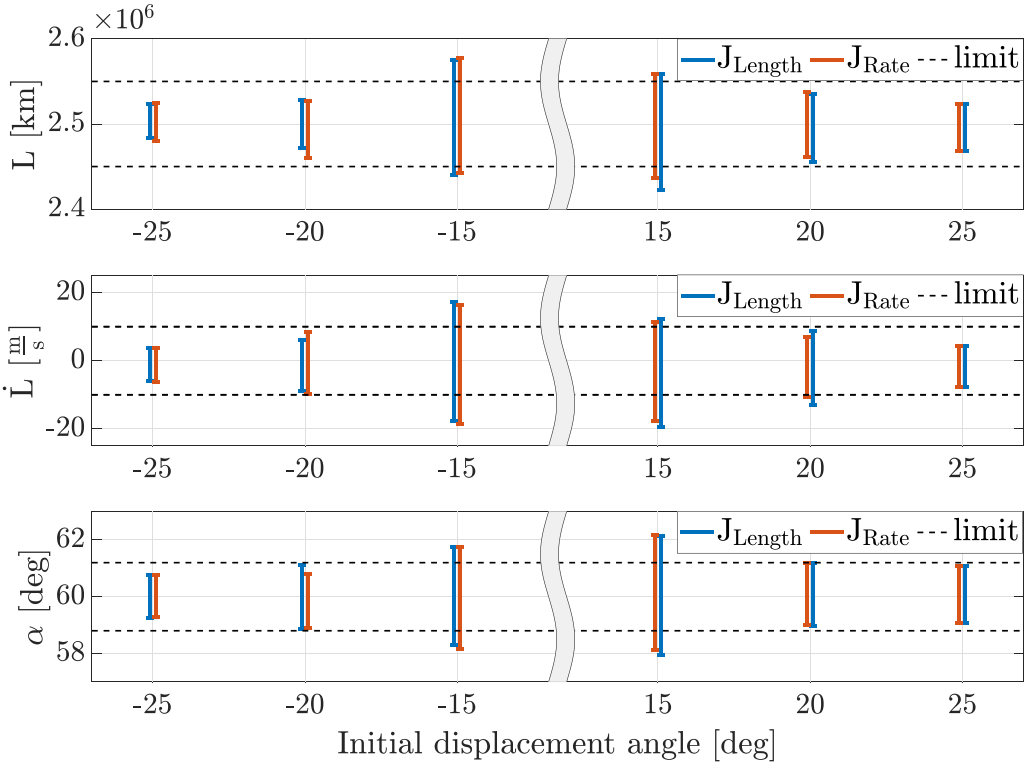

Fig. 9. Comparison of optimized solutions with the two alternative cost functions for different initial displacement angles.

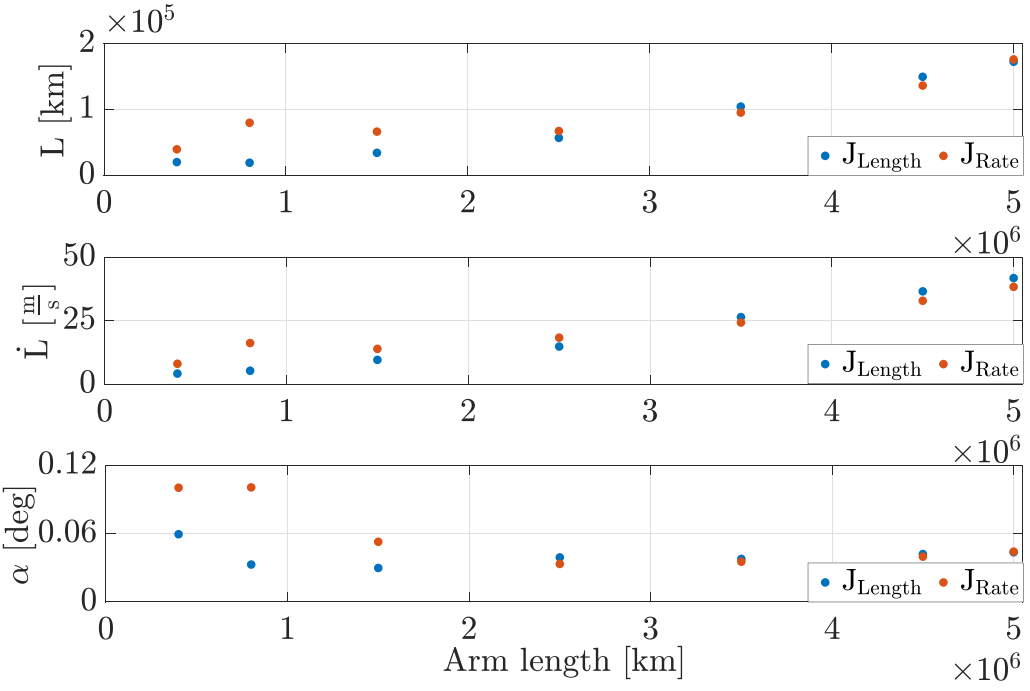

Fig. 10. Maximum variation comparison between J_{Length} and J_{Rate} for different arm lengths.

observed that for arm lengths equal to or less than 2.5 million kilometers, J_{Length} yields better results. Conversely, for arm lengths exceeding 2.5 million kilometers, the two cost functions generate almost comparable outcomes, with slightly better performance observed for J_{Rate}.

4. Preliminary transfer design and optimization

The transfer from Earth to the cartwheel orbit insertion is achieved using a direct injection, with the strict constraint that all three spacecraft must be launched simultaneously using a single launcher. This initial phase involves all satellites travelling along the same path, leveraging the single launch vehicle to deploy all spacecraft to a common initial trajectory, from which they can then manoeuvre to their respective orbit. To simplify the transfer problem the trajectory is divided into two parts — a hyperbolic escape from parking orbit up to Earth's SOI and a heliocentric transfer from SOI to the final science orbits — with a total time of flight expected to be around one year. While the total transfer time was not set as a strict constraint, a 2-month range was imposed on the flight duration to reduce the solution space and maintain flexibility in the optimization process. During the transfer phase, the trajectory files resulting from the science orbit optimization (as described in the previous section) files serve a crucial purpose in providing precise state vectors at specific epochs. These files document the position and velocity of the spacecraft during the science phase, enabling the optimization of the transfer trajectory to align with these states. This integration ensures a connection between the transfer and science phases. Two distinct strategies have been developed to optimize the manoeuvres and the asymptotic conditions in order to obtain the hyperbolic escape and the heliocentric trajectory by propagating the trajectories backward and forward, respectively and are presented in the following subsections. Note that the optimization framework described below could be extended to include an arbitrary number of impulsive manoeuvres. As a final note is worth noting that the results that will be presented in the following sections were obtained using a non-gradient based solver, specifically (COBYLA). This a necessary choice due to the complexity of the optimization problem, which rendered gradient-based methods impractical.

4.1. First strategy - single injection

The optimisation process involves several variables, including the time instants at which each spacecraft deviates from the initial injection trajectory, the ΔV of each manoeuvre and the asymptotic conditions of the velocity vector, composed of the magnitude v_∞, infinite right ascension α_∞, and infinite declination δ_∞. These parameters are defined in a reference frame where the origin is in the center of the Earth, the x-axis points towards the vernal equinox,

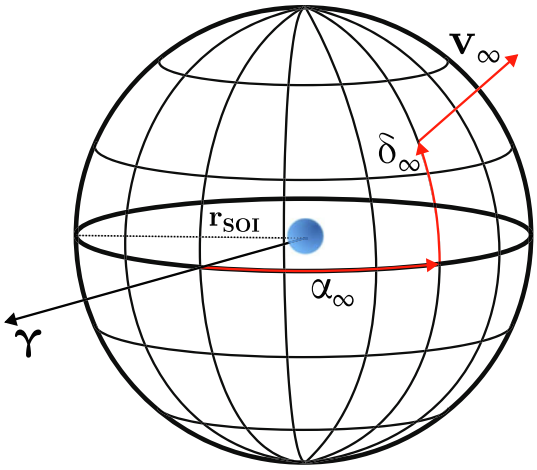

Fig. 11. Infinite coordinate reference frame.

the y-axis lies in the equatorial plane and is orthogonal to the x-axis, and the z-axis points towards the north celestial pole. Specifically, v_∞ represents the asymptotic speed of the spacecraft relative to Earth as it exits the SOI, α_∞ is the angle measured eastward along the celestial equator from the vernal equinox to the projection of the spacecraft's velocity vector onto the equatorial plane, and δ_∞ is the angle between the spacecraft's velocity vector and the celestial equator as shown in Fig. 11. It is worth noting that to reduce the complexity of the optimization process, the position on the sphere of influence is not subjected to optimization. Instead, it can be defined from $\mathbf{v}_\infty$ by fixing the perigee and inclination of the departing hyperbola. The first strategy aims to simplify the problem by optimizing each spacecraft's trajectory individually. This is achieved using a shooting function between two trajectories: the final science orbit, stored into orbit files and loaded into memory, and the injection trajectory, which is unknown and must be optimized. The overall strategy can be summarized as follows:

1. Compute the injection trajectory by optimizing the infinite conditions to minimize the cost of the insertion manoeuvre with Eq. (22).
2. Select the reference trajectory from the ones just optimized to be used as the common trajectory.
3. Use Eq. (23) to re-optimize the remaining trajectories from the shared initial trajectory to the final orbit.

This strategy involves two distinct optimization phases. The initial optimization focuses on determining the transfer trajectory for the spacecraft, which will perform only a final manoeuvre to insert itself into the science orbit. This optimization aims to minimize the final ΔV required, as the initial ΔV is assumed to be provided by the launch vehicle, which places only one of the spacecraft on the correct transfer trajectory. In this initial step the satellites are treated as individual objects with no constraints between them, departing from the SOI with the launcher-defined

conditions. Eq. (22) aims to compute the initial injection trajectory by determining three potential paths based on the conditions at infinity, the initial time at which the satellite is on the SOI and the arrival time at the cartwheel orbit. The cost function consists of the final ΔV only, since the initial one is given by the launcher, but to avoid relying too much on the launcher performances v_∞ is bounded to 500 m/s. This optimization problem produces three different trajectories leading each spacecraft from the SOI to their science orbit, indicated with $(\cdot)^s$.

The transfer solutions are obtained by solving the following NLP problem:

$$\min_{\mathbf{y}_1} \ \Delta V_f \qquad \text{subject to } \mathbf{r}(t_f) = \mathbf{r}^s(t_f) \qquad \text{where } \mathbf{y}_1 = [v_\infty, \alpha_\infty, \delta_\infty, t_i, t_f] \tag{22}$$

The second optimization phase start by selecting the trajectory with the earliest initial time as the reference orbit common for all the three spacecraft since it will ideally contains the optimal releasing times of the other two units. This is valid only if the initial time computed in Eq. (22) and the releasing time are relatively similar. These spacecraft will follow the initial path determined in the first optimization but will require two manoeuvres: an initial one to correct their transfer trajectories and a final one to achieve their science orbit. The two satellites whose trajectories were not selected as reference injection trajectory are re-optimized using the optimization method stated in Eq. (23):

$$\min_{\mathbf{y}_2} \ \Delta V \quad \text{subject to } \mathbf{r}(t_f) = \mathbf{r}^s(t_f) \qquad \text{where } \mathbf{y}_2 = [t_i, t_f, \Delta \mathbf{V}_i] \tag{23}$$

The decision vector for this problem comprises the releasing time (t_i), the arrival time (t_f) and the vectorial components of the initial ΔV while the objective function is the sum of the initial and final delta-vs. In contrast to the optimization of the shared initial trajectory, both delta-Vs are taken into account, since after the same initial orbit the other two spacecraft have to change their initial trajectory to reach the final scientific orbit.

The proposed strategy involves optimizing the launcher's infinite conditions that are optimal for a single satellite, meaning that no manoeuvres close to the SOI are needed. This single satellite trajectory is used as initial common trajectory from which the other two spacecraft departs to reach their final orbit. This approach breaks the transfer into smaller segments, making the computational process more manageable. However, solving five optimization problems, three to obtain the reference trajectory and two to re-optimize the missing satellites, can be time-consuming nullifying the advantage of having approached each satellite singularly. A major disadvantage of this strategy is that the satellite injected directly by the launcher will always have a lower ΔV than the others. This can limit the mission in terms of operational lifetime due to the different amount of fuel in each spacecraft. To mitigate this, the satellite with more fuel shall perform more frequent trajectory correction during the science phase, partially solving the problem of having different transfer costs but possibly increasing the complexity of mission management during the operational phase. To optimize the transfer and determine the optimal initial and final time, a search space must be defined. A preliminary analysis was conducted to assess the cost of the transfer from the mean Earth (i.e, assuming that the Earth orbit has eccentricity $e = 0$) to the final science orbit, revealing, for the optimal ΔV, a time of flight of 11 months, deemed an acceptable duration (see Table 4). For the specific example in this section, the initial and final guessed dates are respectively:

t_i= 2031–05-01T00:00:00 TDB
t_f = 2032–04-01T00:00:00 TDB

with a two month window centered on these epochs. The final results obtained after reoptimizing the two satellites are presented in Table 5.

Table 4
Optimized results obtained solving the problems presented in Eqs. (22) for the Single Injection strategy.

	ΔV [km/s]	t_i [TDB]	t_f [TDB]
SC$_1$	1.041	2031–05-28T09:50:58	2032–03-30T17:24:08
SC$_2$	0.837	2031–05-12T16:07:23	2032–03-28T09:35:08
SC$_3$	0.564	2031–04-27T18:05:45	2032–03-25T23:52:13

Solving Eq. (22) reveals that the first spacecraft to reach the SOI is SC$_3$, released from the launcher on an optimal trajectory directly towards the science orbit, without requiring an initial manoeuvre. The other two spacecraft need to be re-optimized following Eq. (23), inserting the required initial and final manoeuvres to reach the desired target orbit. The transfer total cost, defined as the sum of the ΔV of each spacecraft, is 2.442 km/s, unequally distributed between the three spacecraft. As expected, the ΔV of the satellite directly injected on the target trajectory is lower than the others, with ΔV_3 being approximately half of ΔV_1. As outlined before, this difference could impact the design and sizing of the satellite bus, departing from an homogeneous formation, and possibly management of the operational phase.

4.2. Second strategy - multiple injection

The second strategy aims to optimize the transfer problem by simultaneously optimizing the common initial trajectory and the three satellites, considering three different epochs at which each spacecraft leaves the common orbit. Fig. 12 provides a graphical interpretation of the strategy, showing that the three spacecraft initially follow the same trajectory, optimal for all the units of the fleet, and each satellite departs from this orbit at different times. An impulsive manoeuvre is performed at separation by each

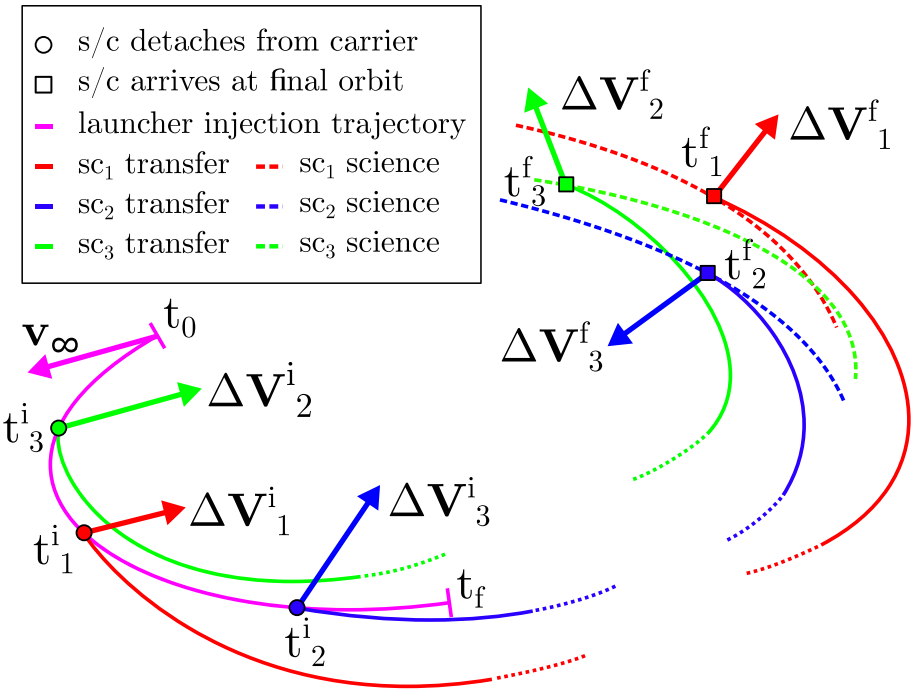

Fig. 12. Diagram of the optimization process used for the Multiple injection strategy.

spacecraft to inject into the transfer orbit. Each spacecraft then performs an impulsive manoeuvre for the insertion in the science orbit.

Unlike the first strategy, the infinite conditions at Earth departure are optimal for all spacecraft rather than for a single unit, resulting in a more evenly distributed total ΔV budget among the fleet. The strategy involves the following steps:

1. Define and propagate the initial conditions of the injection trajectory.
2. Extract the initial conditions of each satellite from the initial common trajectory and propagate up to the final time.
3. Compute the cost function and constraints with the final conditions of the satellites and obtain the three optimized transfer trajectories.

The common initial trajectory, denoted by $(\cdot)^c$, is computed given the conditions at infinite and an initial and final time, t_0 and t_f, which define the propagation limits of the shared orbit. To reduce the number of optimisation variables, these time instants are fixed and each unit is constrained to separate from the initial trajectory between t_0 and t_f. Once the common orbit has been calculated, the states of the individual satellites can be extracted at their respective departure times. The satellite's position is determined by its location on the initial injection orbit, while its velocity is calculated as the velocity of the initial injection orbit adjusted by the initial manoeuvre, ΔV_i. The last step involved propagating the satellites up to the final time and computing the cost function and constraints to match the final positions with the science orbits stored in the orbit files. The formulation of this optimization problem is presented in Eq. (24).

$$\min_{\mathbf{y}_2} \ (\Delta \mathrm{V}_1 + \Delta \mathrm{V}_2 + \Delta \mathrm{V}_3) \qquad \text{subject to} \begin{cases} \mathbf{r_1}(t_f) = \mathbf{r_1^s}(t_f) \\ \mathbf{r_2}(t_f) = \mathbf{r_2^s}(t_f) \\ \mathbf{r_3}(t_f) = \mathbf{r_3^s}(t_f) \end{cases}$$

$$\text{where} \begin{cases} \mathscr{X}_1 = [t_{1,i}, t_{1,f}, \Delta \mathbf{V}_{1,i}] \\ \mathscr{X}_2 = [t_{2,i}, t_{2,f}, \Delta \mathbf{V}_{2,i}] \\ \mathscr{X}_3 = [t_{3,i}, t_{3,f}, \Delta \mathbf{V}_{3,i}] \\ \Delta \mathrm{V}_1 = \Delta \mathrm{V}_{1,\mathrm{i}} + \Delta \mathrm{V}_{1,\mathrm{f}} \\ \Delta \mathrm{V}_2 = \Delta \mathrm{V}_{2,\mathrm{i}} + \Delta \mathrm{V}_{2,\mathrm{f}} \\ \Delta \mathrm{V}_3 = \Delta \mathrm{V}_{3,\mathrm{i}} + \Delta \mathrm{V}_{3,\mathrm{f}} \end{cases} \tag{24}$$

Table 5
Optimized results obtained solving the problems presented in Eqs. (23) for the Single Injection strategy.

	$\Delta \mathbf{V_i}$ [km/s]	$\mathbf{az_i}$ [rad]	$\mathbf{el_i}$ [rad]	$\Delta \mathbf{V_f}$ [km/s]	$\mathbf{az_f}$ [rad]	$\mathbf{el_f}$ [rad]
$\mathbf{SC_1}$	0.426	0.977	1.179	0.615	−1.917	−0.242
$\mathbf{SC_2}$	0.068	−0.608	1.176	0.769	−2.183	−0.623
$\mathbf{SC_3}$	–	–	–	0.564	−1.831	−0.080

Table 6
Optimized results obtained solving the problems presented in Eq. 24 for the Multiple Injection strategy.

	ΔV [km/s]	t_i [TDB]	t_f [TDB]
SC_1	0.965	2031–05-15T23:59:14	2032–03-31T21:51:33
SC_2	0.761	2031–05-01T04:51:10	2032–03-19T09:01:35
SC_3	0.735	2031–05-11T15:36:25	2032–04-07T00:47:22

Table 7
Magnitude and direction of the initial and final manoeuvres for the April solution of the Multiple Injection strategy.

	ΔV_i [km/s]	az_i [rad]	el_i [rad]	ΔV_f [km/s]	az_f [rad]	el_f [rad]
SC_1	0.350	0.968	1.050	0.615	1.547	−0.091
SC_2	0.065	−2.953	−0.533	0.696	1.363	0.512
SC_3	0.153	3.051	−1.240	0.582	1.432	−0.090

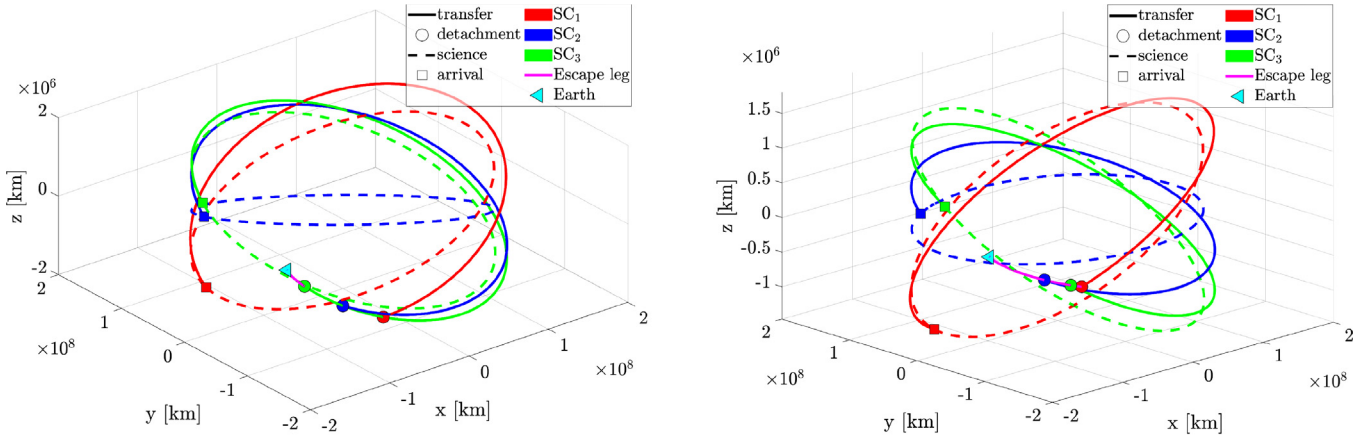

(a) Single Injection strategy

(b) Multiple Injection strategy

Fig. 13. Heliocentric trajectory showing both transfer and science phase.

The results of the second transfer strategy are easier to interpret as they involve a single optimization carried out in an epoch comparable to that of the first strategy, thus ensuring a fair comparison between the two methods. Once the initial time for the injection trajectory has been established, which in this case is $t_0 = 2031–04-16T00:00:00$ TDB.

The next step involves defining the release times for the three satellites, selected in the time interval $[t_0;\ t_0 + 35]$ days. The results for the Multiple Injection strategy are presented in Table 6 and in Table 7, with a total cost of 2.460 km/s.

5. Strategy comparison

In this section the two transfer strategies are compared. First, the two transfer phases are analysed in terms of overall cost and evolution of the formation geometrical parameters. The evolution of the orbital elements throughout the transfers are then provided, followed by an analysis to characterise the effect of the launch date on the total mission cost to identify seasonal trends.

5.1. Transfer cost and parameters analysis

The Single and Multiple Injection Strategies introduced in Sections 4.1 and 4.2 are here compared. The transfer phase trajectories are represented in Fig. 13 as solid lines, together with the target science orbits (dashed lines). The two-impulse transfer in both cases shall result in a rephasing and inclination change to acquire the target orbital state on the previously optimized target science orbit. For the single injection, SC 3 is injected directly in the proximity of the target orbital plane (Fig. 13a) hence its lower delta-V. The higher delta-V of SC 1 is instead explained by the need to perform the largest inclination change among the three spacecraft. Note that the selection of the common initial trajectory is done according to the minimum insertion cost among the three spacecraft. This might

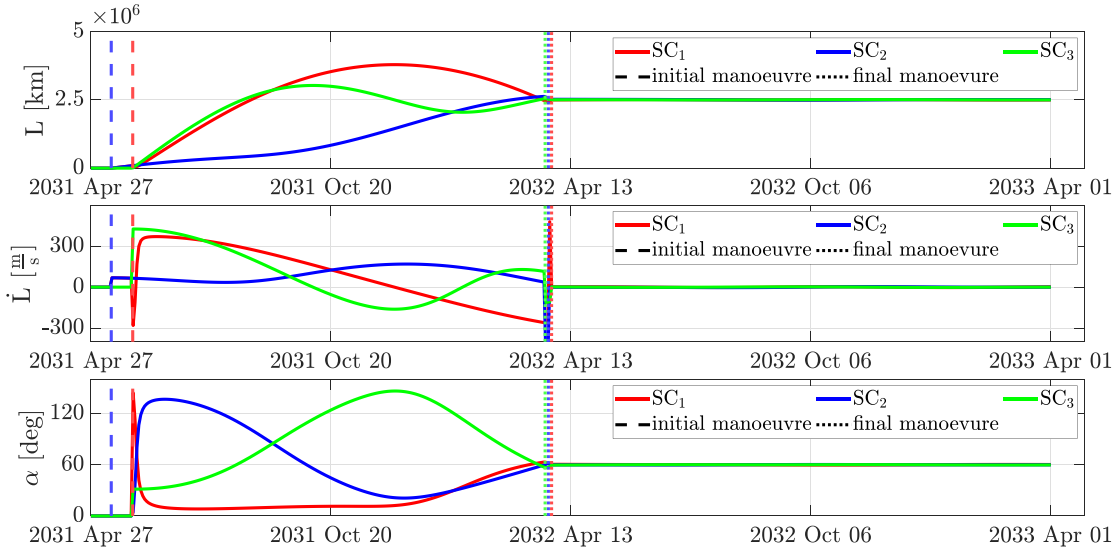

(a) Single Injection strategy

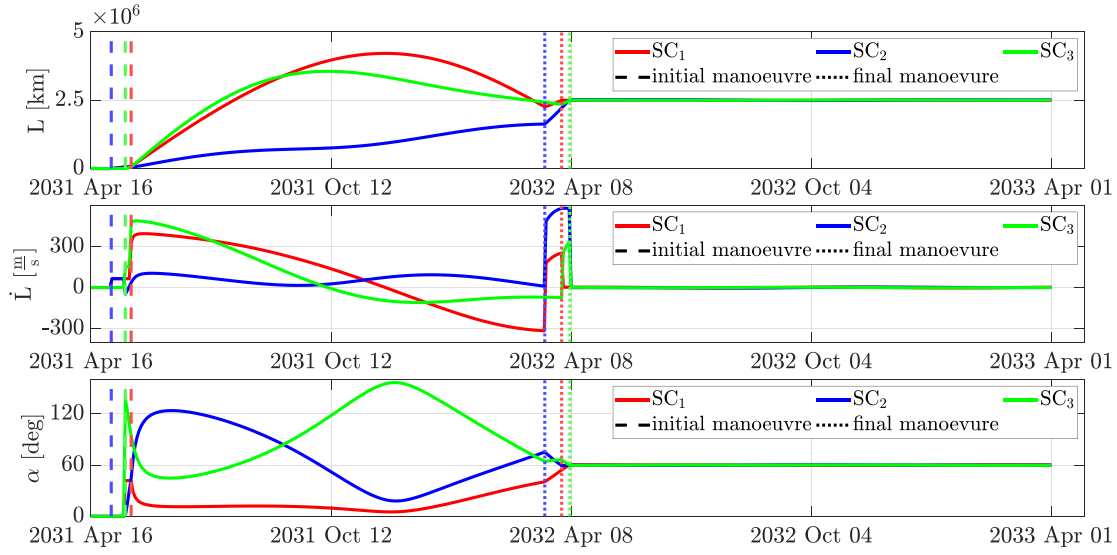

(b) Multiple Injection strategy

Fig. 14. Evolution of the geometrical parameters $L, \dot{L}$ and α with manoeuvres in both transfer and science phase.

result in higher costs for plane change manoeuvres if the difference in inclination is the highest among two orbits. For the Multiple Injection strategy, despite the similar delta-V among the three spacecraft, it can be observed that the optimized manoeuvres have different effects: For SC1 and SC3 the first manoeuvres produces an inclination change which puts them in proximity of the target orbital plane, while for SC2 the inclination change is obtained with the second manoeuvre.

The evolution of the arm length L, arm length rate $\dot{L}$, and corner angle is instead given in Fig. 14. The arm length is zero before the first spacecraft separation and reaches the target value after the final manoeuvre, as expected from the optimization. Despite the different approaches, is interesting to observe a similarity in the behaviour of the arm length L in the transfer phase for both strategies. From the plots it can be also noted that the Single Injection results in a similar target orbit arrival for all three spacecraft, while for the Multiple Injection there is a 20 days delay between SC2 and SC3 arrival.

The results presented indicate that the second strategy is more suitable for the mission design of having all identical satellites while maintaining a similar cost compared to the first strategy. The overall cost of the two transfers are 2.442 km/s and 2.460 km/s for the first and second approach, respectively. Although the latter is slightly higher, the advantage lies in the cost distribution within the satellites of the formation. The maximum difference in the *Multiple injection* strategy is only 200 m/s, while for the first one it is around 500 m/s. This confirms the beneficial effect of the launcher's choice of an initial injection orbit that is intermediate between the three satellite trans-

fer orbits, with the advantage of having the same number of manoeuvres (one separation and one insertion manoeuvre each) and a total cost comparable to single injection strategy. However, the main disadvantage the multiple injection is its computational intensity since it requires calculating an optimal solution for a set of 19 optimization variables. The launcher may still inject the three spacecraft into a heliocentric orbit that is more favorable in terms of ΔV for one unit over another, but this is not embedded in the problem formulation as in the first strategy.

5.2. Orbital elements evolution

It is also possible to compare the two strategies in terms of evolution of the orbital elements, which helps visualizing the effect of the manoeuvres and the differences in the two strategies. The evolution of the orbital elements of the three spacecraft for the *Single Injection* strategy is represented in Fig. 15. SC3 performs only one manoeuvre, which circularizes the orbit and provides the target inclination. The change in RAAN is the smallest among the three spacecraft. For SC1, the first manoeuvre corrects mainly the eccentricity and RAAN, while for SC3 the effect is more in terms of inclination. The second manoeuvre is instead acting on the other orbital elements, i.e., inclination for SC1 and RAAN and eccentricity for SC2. Fig. 16 presents the same plot for the *Multiple Injection* strategy. With respect to the previous case, it can be observed that all manoeuvres act on the inclination for all three spacecraft and the first manoeuvre is not changing the semi-major axis. The second manoeuvre instead circularizes the orbit and allows reaching the target semi-major axis. By comparing the two results, a similar evolution of the eccentricity and RAAN can also be observed.

5.3. Launch date analysis

The Multiple injection strategy is then analysed more extensively by computing the cost for different departing epochs, moving the t_0 by one month covering an entire year. The cost of the mission exhibits a variation along the year, but remains bounded between 2.5 km/s and 3.2 km/s. By examining the trend of ΔV as shown in Fig. 17, two local minima are identified, one in April (lower cost among all considered solutions) and one in October-November. The analysis shows a varying behaviour regarding the ΔV associated to each spacecraft, with cases in which the cost is almost identical between the three satellites and cases in which the costs is not so evenly distributed. Although this strategy does not systematically prevent optimal solution characterized by major differences in ΔV, this phenomenon is largely mitigated and still smaller than in the Single injection strategy. It is worth noting that the ΔV distribution has a larger difference for the November solution, with a cost of 1154 m/s for SC2, 850 m/s for SC1 and 589 m/s for SC3. This also corresponds to the highest single Δv among all solutions. Indeed, the largest cost per single spacecraft ranges from the above cited maximum in November to a minimum of 965 m/s in April as can be seen in Fig. 17.

A more in-depth comparison can be made with the results presented in (Martens and Joffre, 2021) for a specific case study in February 2034. In that case, a ΔV budget of approximately 1092 m/s per spacecraft was estimated using Solar Electric Propulsion (SEP) and Trajectory Correction Manoeuvres (TCMs). It is crucial to highlight that these two elements differentiate the analyses, as this work considers a transfer using chemical propulsion and does not introduce TCMs. Despite these differences, the results obtained in other works align with the estimates obtained with the proposed approach, with an overall ΔV ranging between 2.5 km/s to 3.2 km/s throughout the year, with the specific case of February being slightly lower of 3 km/s for the whole fleet.

The reference cartwheel formation considered for this work is close to the one of LISA both in terms of geometry and positioning with $L = 2.5\text{e}6$ km and $\Theta_0 = -20$ deg. Although the considered mission profile, launch date, and

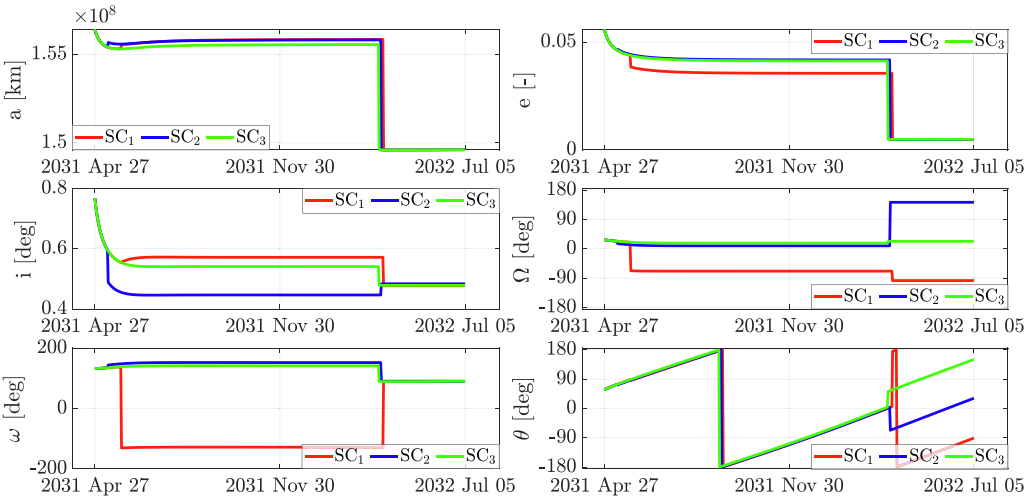

Fig. 15. Orbital element evolution during transfer and first part of science phase for *Single Injection* strategy.

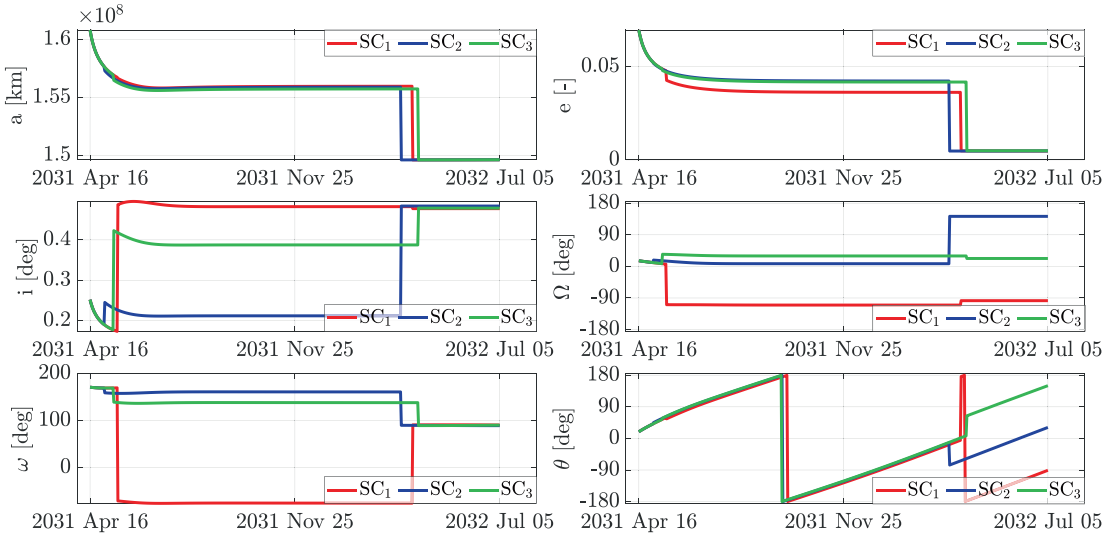

Fig. 16. Orbital element evolution during transfer and first part of science phase for *Multiple Injection* strategy.

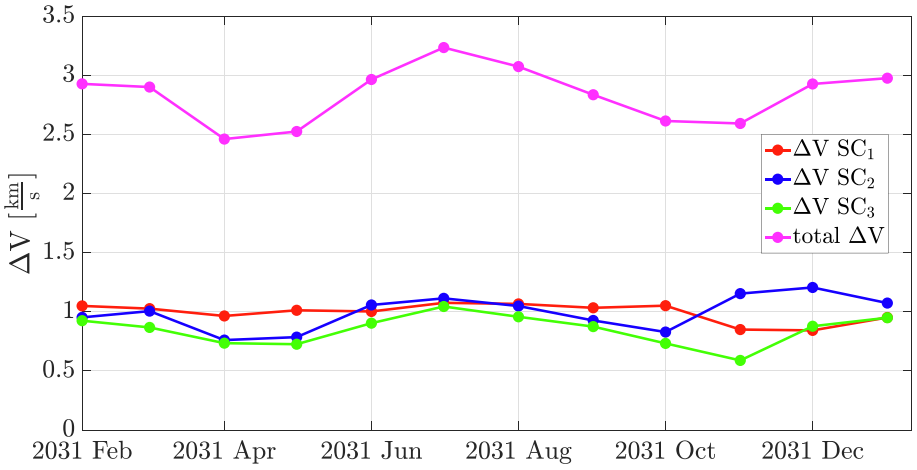

Fig. 17. ΔV trend for an entire year obtained with the *Multiple Injection* strategy.

operative scenario have some fundamental differences with LISA, it is still possible to compare the overall cost over a one-year time window. The total ΔV for LISA in a year ranges between 2.0 and 3.0 km/s, while for this analysis the overall cost is slightly higher and comprised between 2.5 and 3.4 km/s. The disparity in the total time of flight for the two missions can provide an additional explanation for this variation. Specifically, the time of flight for LISA varies between 440 and 540 days as found in (Martens and Joffre, 2021), while for the proposed strategy it ranges between 320 and 370 days.

6. Conclusions

This paper presents a preliminary mission design for a cartwheel formation, focusing on the development of new strategies for acquiring and maintaining the fleet in a perturbed dynamic environment. The approach presented employs two stages.

First, an optimization strategy to determine the set of optimal initial orbital elements which guarantee stability of the cartwheel formation during the science phase is presented. Even in presence of SRP, the optimized initial conditions are capable of maintaining, for the whole mission duration, the relative positions between the individual spacecraft within the target upper and lower bounds. Two alternative objective functions were considered, one controlling the arm-length and the other the arm-length rate. For both objective functions, the optimization process could successfully minimize formation geometry variations, hence limiting the breathing motion of the formation. The choice between the two cost functions depends on the initial conditions, arm length and initial displacement angle. It is also worth noting that with an initial dis-

placement greater than 20 deg the need of station keeping manoeuvre during the science phase is greatly reduced.

Secondly, an optimization strategy tailored for the transfer phase is presented. The release conditions and the escape asymptote are optimized together with a maximum of two impulsive manoeuvres per spacecraft. Two different approaches are considered for the injection. The Single Injection strategy selects the Earth escape direction which is optimal for one of the three spacecraft, hence removing the need for a manoeuvre for the element of the fleet directly released on its optimal route. The Multiple Injection strategy, instead, selects a release asymptote which is average for all the three spacecraft, resulting in a more homogeneous distribution of the ΔV among the fleet. The second strategy is more suitable in case of standardized platform, since the mass budget would be similar for all three spacecraft.

More convoluted optimization strategy are foreseen to further explore the possibility of performing the acquisition and maintenance of deep-space cartwheel formations. In particular, other options beyond the direct injection approach can be considered, mainly determining escape trajectories which could leverage on lunar perturbations or low-energy transfers through the Sun-Earth Lagrangian points (Dei Tos et al., 2019). Additionally, a unified optimization framework which considers at the same time both the transfer and science phase could potentially reduce the overall cost, with the drawback of an increased computational burden. In this latter case, multi-objective optimization with cost functions and constraints tailored for the transfer and cartwheel acquisition phases shall be devised and tuned.

Declaration of Competing Interest

The authors declare that they have no known competing financial interests or personal relationships that could have appeared to influence the work reported in this paper.

References

Alfriend, K.T., Vadali, S.R., Gurfil, P. et al., 2010a. Chapter 10 - Formation Control. In: Alfriend, K.T., Vadali, S.R., Gurfil, P., How, J.P., Breger, L.S. (Eds.), Spacecraft Formation Flying, pp. 241–270. Oxford: Butterworth-Heinemann. doi:10.1016/B978-0-7506-8533-7.00215-3.

Alfriend, K.T., Vadali, S.R., Gurfil, P. et al., 2010b. Chapter 5 - Linear Equations of Relative Motion. In: Alfriend, K.T., Vadali, S.R., Gurfil, P., How, J.P., Breger, L.S. (Eds.), Spacecraft Formation Flying, pp. 83–121. Oxford: Butterworth-Heinemann. doi:10.1016/B978-0-7506-8533-7.00210-4.

Amaro-Seoane, P., Audley, H., Babak, S. et al., 2017. Laser interferometer space antenna. arXiv:1702.00786.

Bandyopadhyay, S., Foust, R., Subramanian, G.P., et al., 2016. Review of formation flying and constellation missions using nanosatellites. J. Spacecr. Rock. 53 (3), 567–578. https://doi.org/10.2514/1.A33291.

Beigelman, I., Gurfil, P., 2008. Optimal fuel-balanced impulsive formationkeeping for perturbed spacecraft orbits. J. Guid., Control, Dynam. 31 (5), 1266–1283. https://doi.org/10.2514/1.34266.

Biscani, F., Izzo, D., 2020. A parallel global multiobjective framework for optimization: pagmo. J. Open Source Software 5 (53), 2338. https://doi.org/10.21105/joss.02338.

Burderi, L., Sanna, A., Di Salvo, T. et al., 2022. ALBATROS & HERMES/SpIRIT: probing space-time quantum foam and hunting for gravitational wave electromagnetic counterparts. In: 44th COSPAR Scientific Assembly. Held 16–24 July, p. 1975. volume 44.

Clohessy, W.H., Wiltshire, R.S., 1960. Terminal guidance system for satellite rendezvous. J. Aerospace Sci. 27 (9), 653–658. https://doi.org/10.2514/8.8704.

Colpi, M., Danzmann, K., Hewitson, M. et al., 2024. LISA Definition Study Report. arXiv:2402.07571.

Contreras, R., Penin, L., Marco, V. et al., 2017. Proba-3 High precision Formation Flying in HEO. In R.R. Rohrschneider (Ed.), Advances in the Astronautical Sciences Guidance, Navigation and Control. volume 159.

D'Amico, S., De Florio, S., Larsson Nordström, R. et al., 2009. Autonomous Formation Keeping and Reconfiguration for Remote Sensing Spacecraft. In: 21st ISSFD.

D'Amico, S., Montenbruck, O., 2006. Proximity operations of formation-flying spacecraft using an eccentricity/inclination vector separation. J. Guid., Control, Dynam. 29. https://doi.org/10.2514/1.15114.

Danzmann, K., & the LISA study team, 1996. LISA: laser interferometer space antenna for gravitational wave measurements. Classical and Quantum Gravity, 13(11A), A247. doi:10.1088/0264-9381/13/11A/033.

Dei Tos, D.A., Rasotto, M., Renk, F. et al., 2019. LISA Pathfinder mission extension: A feasibility analysis. Adv. Space Res., 63(12), 3863–3883. URL: https://www.sciencedirect.com/science/article/pii/S0273117719301565. doi:10.1016/j.asr.2019.02.035.

Escoubet, C., Fehringer, M., Goldstein, M., 2001. The Cluster mission. Ann. Geophys. 19, 1197–1200. https://doi.org/10.5194/angeo-19-1197-2001.

Folkner, W.M., Hechler, F., Sweetser, T.H., et al., 1997. LISA orbit selection and stability. Class. Quantum Gravity, 14(6), 1405. URL: doi:10.1088/0264-9381/14/6/003.

Gill, E., D'Amico, S., Montenbruck, O., 2007. Autonomous formation flying for the PRISMA Mission. J. Spacecr. Rock. 44 (3), 671–681. https://doi.org/10.2514/1.23015.

Hughes, S.P., Bauer, F.H., 2002. Preliminary Optimal Orbit Design for the Laser Interferometer Space Antenna (LISA). In: 25th Annual AAS Guidance and Control Conference (Advances in the Astronautical Sciences) (pp. 61–78). volume 111.

Joffre, E., Martens, W., Renk, F. et al., 2018. Astrodynamics techniques for missions towards Earth-Trailing or Earth-Leading Heliocentric Orbits. In: 7th International Conference on Astrodynamics Tools and Techniques (ICATT).

Joffre, E., Wealthy, D., Fernandez, I. et al., 2021. LISA: Heliocentric formation design for the laser interferometer space antenna mission. Advances in Space Research, 67(11), 3868–3879. URL: https://www.sciencedirect.com/science/article/pii/S0273117720306815. doi:10.1016/j.asr.2020.09.034. Satellite Constellations and Formation Flying.

Le Moigne, J., Adams, J.C., Nag, S., 2020. A new taxonomy for distributed spacecraft missions. IEEE J. Select. Top. Appl. Earth Observ. Remote Sens. 13, 872–883. https://doi.org/10.1109/JSTARS.2020.2964248.

Liu, G.-P., Zhang, S., 2018. A Survey on Formation Control of Small Satellites. Proc. IEEE 106 (3), 440–457. https://doi.org/10.1109/JPROC.2018.2794879.

Martens, W., Joffre, E., 2021. Trajectory design for the ESA LISA mission. J. Astronaut. Sci. 68 (2), 402–443. https://doi.org/10.1007/s40295-021-00263-2.

Nayak, K.R., Koshti, S., Dhurandhar, S.V., et al., 2006. On the minimum flexing of LISA's arms. Class. Quantum Gravity 23 (5), 1763. https://doi.org/10.1088/0264-9381/23/5/017.

Pitkin, M., Reid, S., Rowan, S. et al. (2011). Gravitational wave detection by interferometry (ground and space). Living Rev. Relat., 14(1), 5. URL: https://doi.org/10.12942/lrr-2011-5. doi: 10.12942/lrr-2011-5.

Sabol, C., Burns, R., McLaughlin, C.A., 2001. Satellite formation flying design and evolution. J. Spacecr. Rock. 38 (2), 270–278. https://doi.org/10.2514/2.3681.

Schaub, H., Alfriend, K.T., 2001. Impulsive feedback control to establish specific mean orbit elements of spacecraft formations. J. Guid., Control, Dynam. 24 (4), 739–745. https://doi.org/10.2514/2.4774.

Smith, R.S., Hadaegh, F.Y., 2005. Control of deep-space formation-flying spacecraft; relative sensing and switched information. J. Guid., Control, Dynam. 28 (1), 106–114. https://doi.org/10.2514/1.6165.

Tapley, B.D., 2008. Gravity model determination from the GRACE mission. J. Astronaut. Sci. 56 (3), 273–285. https://doi.org/10.1007/BF03256553.

Wang, W., Wu, D., Lei, H., et al., 2021. Fuel-optimal spacecraft cluster flight around an ellipsoidal asteroid. J. Guid., Control, Dynam. 44 (10), 1875–1882. https://doi.org/10.2514/1.G005993.

Xia, Y., Li, G., Heinzel, G. et al., 2010. Orbit design for the Laser Interferometer Space Antenna (LISA). Science China Physics, Mechanics and Astronomy, 53(1), 179–186. URL: https://doi.org/10.1007/s11433-010-0100-7 doi: 10.1007/s11433-010-0100-7.

Xie, X., Jiang, F., Li, J., 2023. Design and optimization of stable initial heliocentric formation on the example of LISA. Adv. Space Res., 71 (1), 420–438. URL: https://www.sciencedirect.com/science/article/pii/S0273117722008201 doi:10.1016/j.asr.2022.08.084.

Yang, C., Zhang, H., 2019. Formation flight design for a LISA-like gravitational wave observatory via Cascade optimization. Astrodynamics 3, 155–171. https://doi.org/10.1007/s42064-018-0042-9.

Yang, J., Zhang, Z., Jiang, F. et al., 2023. Low-energy transfer design of heliocentric formation using lunar swingby on the example of LISA. Aerospace, 10(1). URL: https://www.mdpi.com/2226-4310/10/1/18. doi:10.3390/aerospace10010018.